





Topological Frenkel exciton polaritons in one-dimensional lattices of strongly coupled cavities

J. Andrés Rojas-Sánchez, Yesenia A. García Jomaso , Brenda Vargas, David Ley Domínguez , César L. Ordoñez-Romero, Hugo A. Lara-García , Arturo Camacho-Guardian ,* and Giuseppe Pirruccio[†]
Instituto de Física, Universidad Nacional Autónoma de México, Apartado Postal 20-364, Ciudad de México, Código Postal 01000, Mexico



(Received 5 December 2022; revised 21 February 2023; accepted 28 February 2023; published 13 March 2023)

Frenkel polaritons, hybrid light-matter quasiparticles, offer promise for the designing of new optoelectronic devices. However, their technological implementations are hindered by sensitivity to imperfections. Topology has been raised as a way to circumvent defects and fabrication limitations. Here, we propose a lattice of cavities to realize the one-dimensional Su-Schrieffer-Heeger model (SSH) for topological Frenkel polaritons. By engineering the configuration of the cavities we demonstrate that the SSH topological and trivial phases can be accessed, which we unravel by employing a dual approach based on classical and quantum theories. We study the role of inherent vibron modes and fabrication defects in the robustness of the topological phases of polaritons. Our study demonstrates a simple experimentally realistic setup to realize topological polaritons at room temperature.

DOI: [10.1103/PhysRevB.107.125407](https://doi.org/10.1103/PhysRevB.107.125407)

I. INTRODUCTION

Frenkel excitons have emerged as a successful platform to realize strongly hybridized phases of light and matter at room temperature [1,2]. Experimental breakthroughs have demonstrated the ability to produce many-body phases such as Bose-Einstein condensation [3–6], superfluidity [7], and a variety of effects resulting from exciton-polariton [8,9] and plasmon-exciton-polariton interactions [10–15], including lasing [16–18], polariton parametric emission [19], and oscillation [20,21], among others. The flexibility of these systems permits the polaritonic control of the internal energy levels [22,23], has opened up the field of polaritonic chemistry [24–27], and has encouraged studies beyond the quasiparticle approach of polaritons [28]. The ultimate control of strongly coupled light-matter excitations, paired up with the emerging field of topological photonics, paved the way to the advent of topological polaritonics [29–31]. This may boost technological applications in quantum optical circuits [32], in nonlinear light [33], in chiral and topological lasers [34–36], and in general where high fabrication precision is challenging to reach.

The advances in topological photonics and polaritonics include breakthrough experiments and theories in the context of cavity- and circuit-QED systems [37–41], ring resonator arrays [42–45], photonic crystals [46–52], microwaves [53–56], and metamaterials [57–61] in which many intriguing topological phases have been realized exploiting the light-matter coupling. Perhaps, the canonical one-dimensional (1D) model with nontrivial topological properties is the so-called Su-Schrieffer-Heeger (SSH) chain. SSH models have already been realized and studied in many systems including

plasmonic chains [62–66], waveguide QED [67], radiative heat transfer [68], and polaritons [69–75]. Topological edge states provide an efficient way to create localized polaritonic modes which are protected by their bulk environment. Room-temperature topological systems are of particular interest because their robustness against fabrication imperfections may lead to next-generation polariton-based technologies.

Organic excitons are a promising platform in which to realize topological hybrid phases of light and matter at ambient conditions. At room temperature, besides the main exciton peak, generic organic excitons exhibit vibron modes and a continuum of excitations that modify the quasiparticle character of the polaritons [28]. The interplay between the topological phases and the decoherence sources of the polaritons remains so far fairly unexplored.

Here, we theoretically propose a room-temperature setup for the realization of the SSH model with Frenkel exciton-polaritons in a one-dimensional lattice of stacked nanocavities. We demonstrate that by alternating the width of the mirrors it is possible to obtain both trivial and nontrivial topological polariton phases. For this, we employ a dual approach based on the transfer matrix method (TMM) combined with a tight-binding model for a chain of exciton-polaritons. The TMM, for the appropriate configuration, unveils the emergence of polariton edge states with localized electric field around the edges of the array. Concomitantly, the reflectance spectrum of the stack is found to closely resemble that of an isolated cavity. The correspondence of these branches with the topologically protected states of the SSH model is demonstrated by means of the tight-binding formalism for exciton-polaritons. Our twofold approach is general and provides a comprehensive tool that enables a deep understanding of the fundamental aspects of stacks of strongly coupled cavities. We discuss the role of the vibron mode and the effects of typical lattice imperfections on the topological phases. We show that the system is robust to fabrication imperfections;

*acamacho@fisica.unam.mx

†pirruccio@fisica.unam.mx

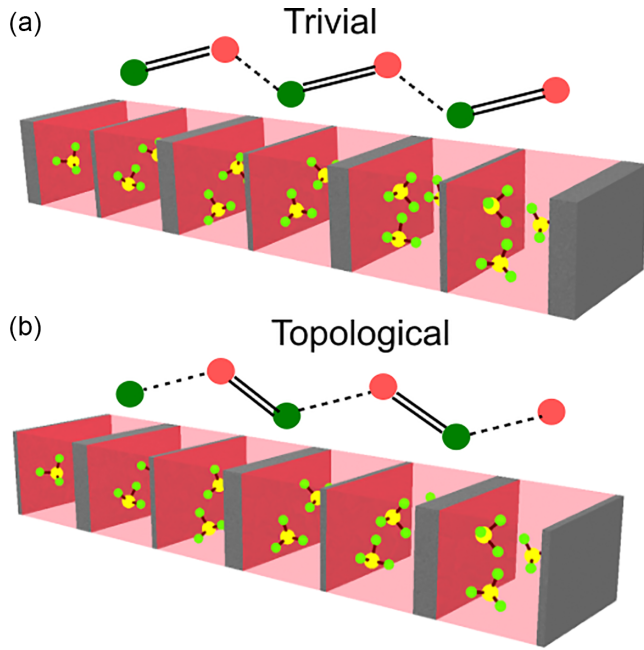


FIG. 1. Schematic representation of the array of $2N$ stacked cavities filled with an organic material and its analogy to the 1D SSH model. Each cavity supports Frenkel exciton-polaritons. The different couplings found in the SSH model are realized by alternating the width of the mirror separating each active layer. (a) Trivial and (b) topological configuration.

however, the topological edge states are sensible to the breakdown of the quasiparticle picture.

In addition, we discuss the experimental implementation of our proposal and its robustness against typical fabrication limitations. Even though we mainly deal with Frenkel polaritons, our formalism is applicable to exciton-polaritons in inorganic materials. This is demonstrated in Sec. VI, where we consider homogeneously broadened excitons lacking vibronic coupling.

Our proposal can be implemented in a wide family of organic polaritons at room temperature and provides therefore a valuable guide for future experiments and theories. An additional value of our proposal stems from the simple and inexpensive fabrication process combined with a simple and scalable design.

II. SYSTEM

Our system consists of an array of $2N$ stacked nanocavities, as illustrated in Fig. 1. All cavities are loaded with a polymer matrix mixed with a highly concentrated organic molecule. In Fig. 2 we show the imaginary part $\kappa(\omega)$ of the refractive index for a generic organic molecule. It is formed by a principal electron transition, associated with the zero-phonon exciton line, strongly coupled to a vibronic sideband. In a typical organic molecule at room temperature, the vibronic shoulder is slightly detuned from the main peak and yet overlaps with it giving rise to a continuum of material excitations that cannot be disentangled. The cavity length L_c , common to all cavities, is such that the fundamental optical mode is zero detuned from the main exciton energy at normal incidence. The width

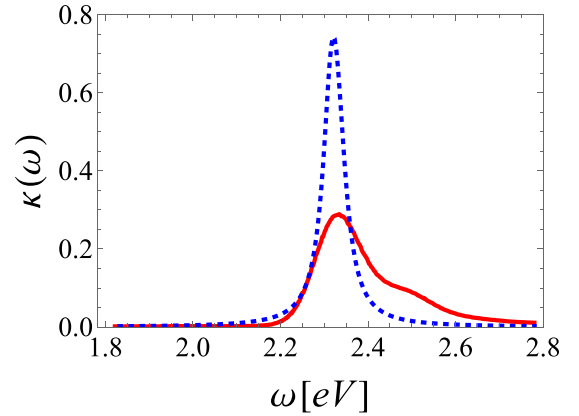


FIG. 2. Imaginary part of the refractive index. The solid red curve represents the spectrum of a typical organic molecule with a principal peak at $\omega_X \approx 2.32$ eV and a second vibron mode around $\omega_S \approx 2.5$ eV. The dashed blue curve represents an ideal exciton with an oscillatory strength of $2\Omega = 0.33$ eV that peaks at $\omega_X = 2.32$ eV and an exciton linewidth of $\gamma_X = 0.025$ eV.

of the metallic mirrors alternates, as depicted in Fig. 1. Two configurations are possible.

The *trivial* configuration, shown in Fig. 1(a), consists of an array of cavities where the odd mirrors have a width of $L_{M,\text{odd}}$ whereas the even mirrors' width equals $L_{M,\text{even}}$, with $L_{M,\text{odd}} > L_{M,\text{even}}$. The *topological* array is obtained by switching the order of the mirrors.

Intuitively, we expect that cavities separated by a thin mirror couple more efficiently than those distanced by a thicker mirror. Thus the trivial configuration allows for the effective coupling of the cavities by pairs, as in the trivial phase of the SSH model. On the other hand, for the topological configuration, only the internal cavities of the stack couple efficiently, whereas the two cavities at the edges of the array appear *isolated*, as in the topological phase of the SSH model.

Our proposal is completely general and independent of the specific organic molecule employed. However, to highlight the experimental feasibility of our setup, we illustrate our results for a concrete dye-doped polymer. Erythrosine B (ErB) has already proved to be a suitable molecule for the realization of exciton-polaritons at room temperature [28].

III. SSH POLARITONS: A TRANSFER-MATRIX-BASED APPROACH

We start our theoretical study employing the transfer matrix method. This is a simple yet powerful tool to study light propagation in multilayer systems with ideal planar and parallel interfaces [76]. We remark that this formalism is not restricted to planar interfaces and can be adapted to spherical or cylindrical stratified structures [77,78].

Our setup, illustrated in Fig. 1, consists of $4N + 3$ layers: $2N + 1$ silver (Ag) mirrors, $2N$ active layers, and 2 semi-infinite dielectric media at the ends of the lattice. The specific active layer used in the following corresponds to polyvinyl alcohol (PVA) mixed with ErB. Its complex refractive index, $\tilde{n}_{\text{ErB}}(\omega)$, is obtained from experimental measurements [28], and its imaginary part, $\kappa_{\text{ErB}}(\omega)$, is shown in Fig. 2.

presents a main exciton at $\omega_X \approx 2.32$ eV and a secondary peak at $\omega_S \approx 2.5$ eV. Here we take $\hbar = 1$.

Without loss of generality, we consider both of the latter media to be air with $n_{\text{Air}} = 1$. The introduction of a substrate at the end of the array of cavities is straightforward in our formalism and does not play a significant role for large N . Its effect is to slightly change the curvature of the polariton bands, leaving unaltered the topological properties of the system. The Ag complex refractive index, $\tilde{n}_{\text{Ag}}(\omega)$, is taken from the experimental reported values [79].

The length of all the active layers is fixed to $L_c = 140$ nm, and the width of all odd mirrors is L_{odd} , while for all even mirrors it is L_{even} . Plane waves propagating in each layer indexed by l are described by an electric field $E_l(z) = A_l e^{ik_l z} + B_l e^{-ik_l z}$. Here, $l = 0$ denotes the first medium (air); for the mirrors and the active layers we have $4N + 2 > l > 0$, where, for an odd l , light propagates in a mirror, while for an even l it propagates in an active layer. Finally, A_l and B_l are the amplitude coefficients for the incoming and outgoing electric fields in each medium. We write the amplitudes in vectorial form, $\mathbf{v}_l = [A_l, B_l]^T$, and connect the coefficients via Maxwell equations and the appropriate boundary conditions. For s -polarized waves and light propagating from the l th to the $(l + 1)$ th medium we obtain $\mathcal{D}_l \mathbf{v}_l = \mathcal{D}_{l+1} \mathbf{v}_{l+1}$. Here, the dynamical matrix \mathcal{D}_l is given by

$$\mathcal{D}_l = \begin{bmatrix} 1 & 1 \\ n_l \cos \theta_l & -n_l \cos \theta_l \end{bmatrix}. \quad (1)$$

Through medium l , the phase changes by

$$\mathcal{P}_l = \begin{bmatrix} e^{i\phi_l} & 0 \\ 0 & e^{-i\phi_l} \end{bmatrix}, \quad (2)$$

where $\phi_l = k_z^l L_l$, L_l is the length of the medium, and k_z^l is the perpendicular component of the wave vector of the electric field and it is given by

$$k_z^l = \frac{\omega}{c} n_l \cos \theta_l \quad (3)$$

with θ_l being the angle of incidence of the light field in the l th medium measured from the z axis, i.e., normal to the stack.

It is convenient to introduce

$$\mathcal{M}_l = \mathcal{D}_l \mathcal{P}_l \mathcal{D}_l^{-1},$$

to write the total transfer matrix \mathcal{T} as

$$\mathcal{T} = \mathcal{D}_0^{-1} \left(\prod_{l=1}^{4N+1} \mathcal{M}_l \right) \mathcal{D}'_0, \quad (4)$$

with \mathcal{D}_0 and \mathcal{D}'_0 being the matrices of the interfaces for the air at the ends of the array.

Finally, the reflectance can be calculated as

$$R = \left| \frac{\mathcal{T}(2, 1)}{\mathcal{T}(1, 1)} \right|^2. \quad (5)$$

Single cavity. Before we explore the reflectance for the two configurations shown in Fig. 1, let us recall the reflectance spectrum for a single cavity. Frenkel polaritons in a single cavity were studied experimentally in Ref. [28]. The reflectance spectrum for a single cavity of length $L_c = 140$ nm features two polariton branches (Fig. 3). The lower polariton arises as a

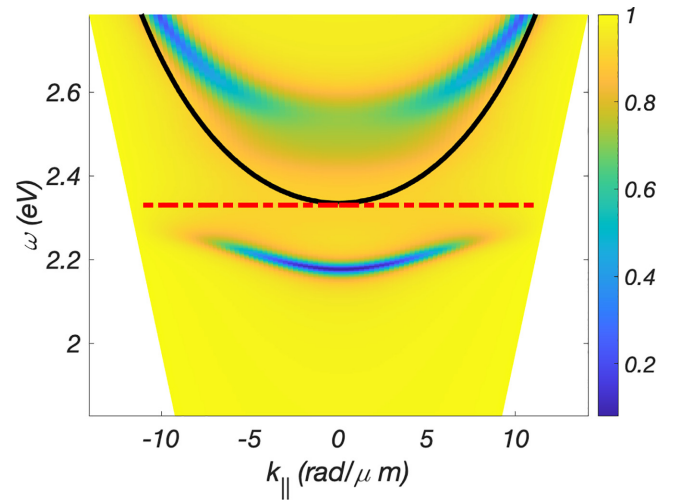


FIG. 3. s -polarized reflectance for a single cavity having $L_c = 140$ nm, $L_1 = 40$ nm, and L_3 semi-infinite. The dashed red line indicates the energy of the bare exciton peak centered around $\omega_X = 2.32$ eV, while the solid black curve corresponds to the bare cavity photon dispersion.

well-defined quasiparticle. Only at large angles, as it becomes purely excitonic, does the reflectance of the lower polariton increase. On the other hand, the upper polariton emerges as an ill-defined polariton at small angles and only becomes a quasiparticle at large angles. As discussed in Ref. [28], the blurring of the upper polariton is an inherent feature of Frenkel polaritons and dramatically influences the quasiparticle character of the polaritons. The separation between the polariton branches at normal incidence is estimated to be around $2\Omega = 0.33$ eV.

Trivial configuration. Let us start discussing the trivial configuration. We take $N = 10$, that is, 20 cavities; the width of all odd mirrors is $L_{\text{odd}} = 30$ nm, while for all even mirrors it is $L_{\text{even}} = 40$ nm. In Fig. 4 we show the reflectance for this configuration as a function of ω and $k_{||} = \frac{\omega}{c} \sin \theta$. Below the energy of the bare exciton, two polariton bands appear

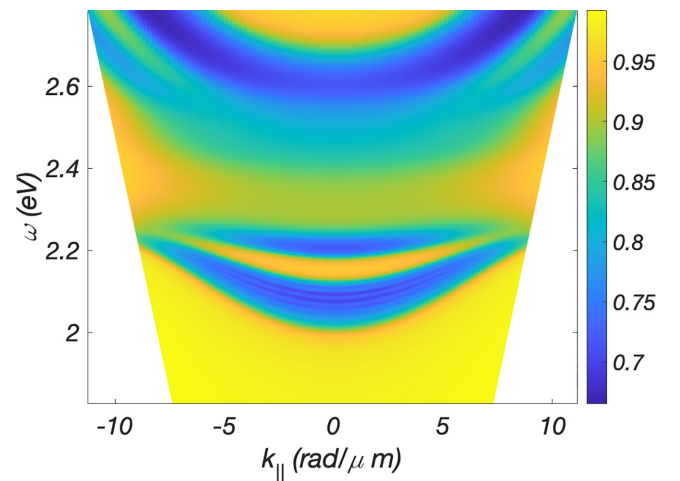


FIG. 4. s -polarized reflectance for the trivial configuration where four polariton bands appear with two band gaps above and below the bare exciton energy.

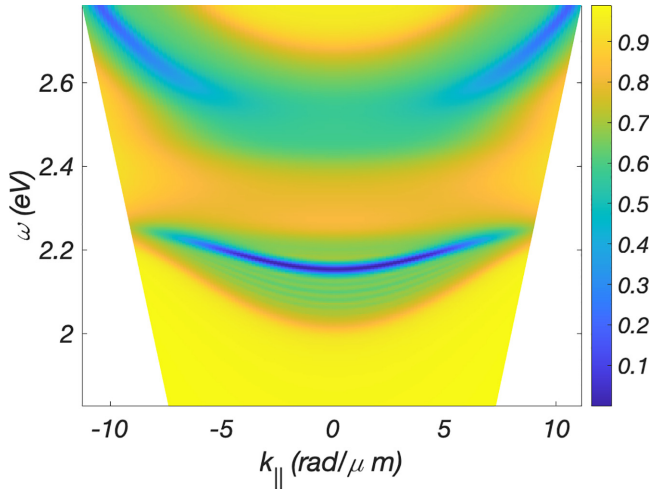


FIG. 5. *s*-polarized reflectance for the topological configuration. Reflectance minima arise within the two band gaps observed for the trivial configuration.

separated by a band gap that becomes maximal at normal incidence and closes for large $k_{||}$ values. In the limit of infinite N , both bands form a continuum. However, for finite N a slight discreteness in the bottom polariton band is expected.

Above the bare exciton energy, two upper polariton bands arise. As a consequence of the vibronic *shoulder* of the exciton absorption, at normal incidence only one of these bands is clearly resolved. For large $k_{||}$, the two upper polariton bands are clearly distinguishable and exhibit a band gap. We note two facts: (i) The band gaps opened by stacking the cavities are smaller than the splitting between the two upper and lower polariton bands, and (ii) these band gaps lie at the spectral position of the polaritons for a single cavity, shown in Fig. 3.

Topological configuration. We now turn our attention to the topological configuration illustrated in Fig. 1(b). The reflectance spectrum obtained from the TMM is shown in Fig. 5 and exhibits striking features compared with the *trivial* configuration. In this case, the reflectance minima are located inside the band gaps found for the *trivial* configuration and closely resemble the upper and lower polaritons of the single cavity, displayed in Fig. 3. Since the upper polariton energy lies inside of the vibronic continuum of excitations, the reflectance spectrum signals an ill-defined upper polariton for small wave vectors. That is, the breakdown of the polariton picture prevents the emergence of a well-defined mode lying inside the band gap above the bare exciton energy. On the other hand, the lower polariton remains well defined for all incident wave vectors.

Looking at the spatial distribution of the normalized electric field intensity, $|E(z)/E_{\max}|^2$, for the topological configuration [shown in Fig. 7(c) as a function of z (blue curve)], we see that the electric field peaks in the odd cavities whereas it significantly drops and essentially vanishes inside the even cavities. The intensity of the electric field in the odd cavities decays exponentially, which further hints at the topological character of our setup.

The TMM strongly suggests that our setup is analogous to the SSH model for exciton-polaritons. However, to explicitly unveil the link with the SSH model, in the following

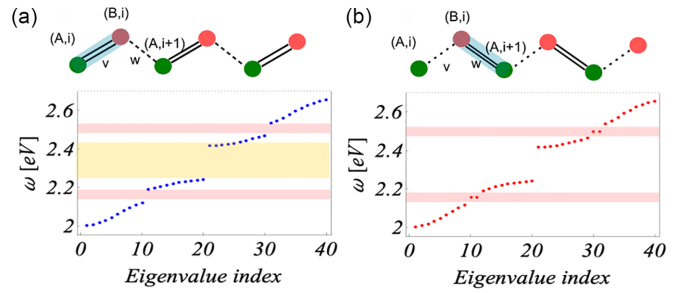


FIG. 6. (a) Eigenvalues for the trivial configuration at normal incidence: four polariton bands corresponding to the two branches of the lower and upper polaritons. Shown at top is a cartoon of the notation employed. (b) Eigenvalues for the topological configuration; inside the energy gaps of the polariton bands, two edge states per branch appear. We take $2N = 20$ cavities giving 40 eigenvalues.

sections we develop a tight-binding model for the exciton-polaritons and contrast it to the TMM.

IV. SSH POLARITONS: AN EFFECTIVE TIGHT-BINDING MODEL APPROACH

The following Hamiltonian describes a set of $2N$ coupled cavities that can be arranged in either the trivial or topological configuration, as illustrated at the top of Figs. 6(a) and 6(b),

$$\begin{aligned} \hat{H} = & \sum_{i=1}^N \omega_c(\theta) (\hat{a}_i^\dagger \hat{a}_i + \hat{b}_i^\dagger \hat{b}_i) + \omega_X (\hat{x}_{i,A}^\dagger \hat{x}_{i,A} + \hat{x}_{i,B}^\dagger \hat{x}_{i,B}) \\ & + \Omega \sum_{i=1}^N (\hat{a}_i^\dagger \hat{x}_{i,A} + \hat{b}_i^\dagger \hat{x}_{i,B} + \text{H.c.}) \\ & - \sum_{i=1}^N (v (\hat{a}_i^\dagger \hat{b}_i + \hat{b}_i^\dagger \hat{a}_i) + w (\hat{a}_{i+1}^\dagger \hat{b}_i + \hat{b}_i^\dagger \hat{a}_{i+1})). \end{aligned} \quad (6)$$

Here, \hat{a}_i^\dagger and \hat{b}_i^\dagger create a cavity photon at sites A and B , respectively, with energy $\omega_c(\theta)$ which depends on the incident angle θ given by the solid black curve in Fig. 3. On the other hand, $\hat{x}_{i,A}^\dagger$ and $\hat{x}_{i,B}^\dagger$ create excitons with site index i in cavities A and B , respectively. Here, the energy of the excitons is ω_X . Excitons and photons couple with a strength Ω only if all site indices are equal. Adjacent cavities couple through the tunneling of photons, where the tunneling amplitude is given by either v or w , depending on the configuration, as illustrated at the top of Figs. 6(a) and 6(b).

We now study the tight-binding model for the exciton-polaritons within the SSH model. For reasons which will become clear later, we take hopping coefficients of $v = 0.15$ and $w = 0.09$ for the trivial configuration, whereas for the topological configuration we simply swap these coefficients, i.e., $w = 0.15$ and $v = 0.09$. The SSH model for exciton-polaritons is a simple quadratic Hamiltonian that can straightforwardly be diagonalized. For consistency with the TMM we take $N = 10$ corresponding to 20 cavities.

Trivial configuration. We start by discussing the trivial configuration. For clarity, we show in Fig. 6(a) the eigenvalues of the Hamiltonian in Eq. (6) considering first normal incidence and resonant conditions $\omega_c(\theta = 0) = \omega_X$. In this case

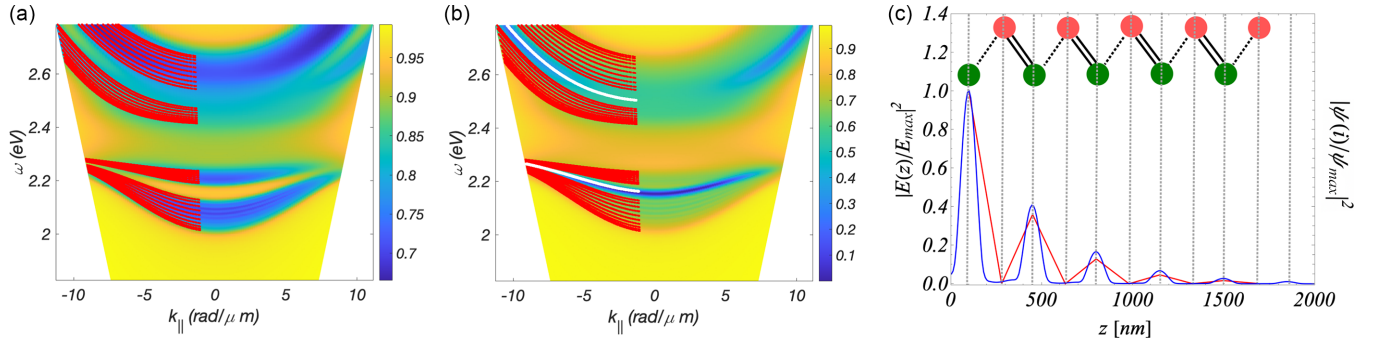


FIG. 7. (a) and (b) Eigenvalues of the SSH model in Eq. (6) as a function of the in-plane momentum k_{\parallel} illustrated by the red dots. The energies of the SSH model are plotted on top of the reflectance spectrum for (a) the trivial configuration and (b) the topological configuration. The white dots are the eigenvalues of Eq. (6) corresponding to edge states and lie at the energies of the bare lower and upper polaritons. (c) Normalized electric field intensity as a function of z (blue curve) and amplitude of the wave function obtained from the SSH model (red curve). The gray vertical lines give the position of the center of the cavities.

we observe that the lower and upper polariton states split leading to four polariton bands: two above and two below the energy of the bare exciton energy. The lower and upper polaritons yield to two bands separated by a gap, marked by the pink area. The Rabi coupling leads to the avoided crossing (yellow area) that separates the lower from the upper polariton bands. These four polariton bands display a difference in their bandwidths. Specifically, the lowest polariton band is broader than the second polariton band. This feature, also visible in the TMM calculations, can hardly be explained within the TMM. Strictly, the information on energy position and width of gaps, resonances, and edge states is encoded in Eq. (5) as discussed for photonic systems in Ref. [52]. However, in our system, the nonanalytical expressions for $\tilde{n}_{\text{ErB}}(\omega)$ and the complex refractive index of the Ag make it highly nontrivial and nonintuitive to retrieve such parameters analytically. Conversely, the tight-binding model provides a very intuitive physical explanation for it. When photons hybridize with excitons forming polaritons, the photon tunneling between adjacent cavities depends on the polaritons' Hopfield coefficients, i.e., the coupling efficiency of polaritons living in adjacent cavities depends on the ratio of their photonic and excitonic components. Thus one expects that polaritons with a large excitonic component exhibit a weak tunneling leading to narrow polariton bands. This is the case for the two bands located around the bare exciton energy. On the other hand, polaritons with a large photonic component lead to a broad bandwidth with the consequence of dispersion and enhanced hopping. In addition, we confirm that the alternating width of the mirrors creates a composite unit cell [80]. This leads to different tunneling coefficients v and w , which in turn gives rise to the two minibands observed both in the TMM and the tight-binding model.

Formally, these arguments can be read by studying the hopping terms of the Hamiltonian. For instance, the tunneling between photons A and B with same site index, i , in the polariton basis ($\hat{L}_{i,\alpha}$, $\hat{U}_{i,\alpha}$) with $\alpha = A, B$ is

$$\begin{aligned}
 -v(\hat{a}_i^\dagger \hat{b}_i + \text{H.c.}) &= -v(\mathcal{S}_{i,A} \mathcal{S}_{i,B} \hat{L}_{i,A}^\dagger \hat{L}_{i,B} \\
 &+ \mathcal{C}_{i,A} \mathcal{C}_{i,B} \hat{U}_{i,A}^\dagger \hat{U}_{i,B} + \mathcal{S}_{i,A} \mathcal{C}_{i,B} \hat{L}_{i,A}^\dagger \hat{U}_{i,B} \\
 &+ \mathcal{C}_{i,A} \mathcal{S}_{i,B} \hat{U}_{i,A}^\dagger \hat{L}_{i,B} + \text{H.c.}). \quad (7)
 \end{aligned}$$

Here, the photon written in the basis of the lower and upper polariton in terms of the standard Hopfield coefficients is $\hat{a}_i/\hat{b}_i = \mathcal{S}_{i,\alpha} \hat{L}_{i,\alpha} + \mathcal{C}_{i,\alpha} \hat{U}_{i,\alpha}$, with $\mathcal{S}_{i,\alpha}^2 + \mathcal{C}_{i,\alpha}^2 = 1$, where

$$\mathcal{C}_{i,\alpha}^2 = \frac{1}{2} \left(1 + \frac{\omega_c(\theta) - \omega_X}{(\omega_c(\theta) - \omega_X)^2 + 4\Omega^2} \right).$$

Equation (7) stresses that adjacent cavity polaritons can only couple via their photonic component. Thus states with very small photonic components have suppressed tunneling and tend to localize within the corresponding cavities. Such localization corresponds to the band flattening observed for the two bands that are close to the bare exciton energy (Fig. 6). In contrast, for states with a large photonic component, the tunneling of polaritons becomes essentially the bare photon term, v , which makes the two polariton bands far detuned from the exciton dispersive and broad.

We remark that an understanding of the narrowing of the bands close to the *bare* exciton line cannot straightforwardly be read from the TMM. This discussion naturally arises from the tight-binding formalism providing a deeper insight into the physical setup.

We can further understand the tight-binding model and its equivalence to the experimental proposal if we vary the incident angle θ . In Fig. 7(a) we plot the eigenvalues of the Hamiltonian (red dots) in Eq. (6) as a function of k_{\parallel} . For clarity in our comparison we show in the background the reflectance spectrum obtained from the TMM. The remarkable agreement between the TMM and the SSH model for exciton-polaritons supports our experimental proposal. Furthermore, we also observe the closing of the lower band gap as the lower polariton becomes more excitonic at larger incident angles, in clear agreement with our previous discussion based on the Hopfield coefficients.

Topological configuration. The topological configuration at normal incidence yields the eigenvalues in Fig. 6(b). In addition to the four polariton bands, we observe the appearance of two edge states located in the middle of the polariton gaps (pink area) whose energy lies exactly at the energy of the polaritons sustained by the single cavity:

$$\omega_{\text{LP/UP}}(\theta) = \frac{1}{2}(\omega_c(\theta) + \omega_X \mp \sqrt{(\omega_c - \omega_X)^2 + 4\Omega^2}). \quad (8)$$

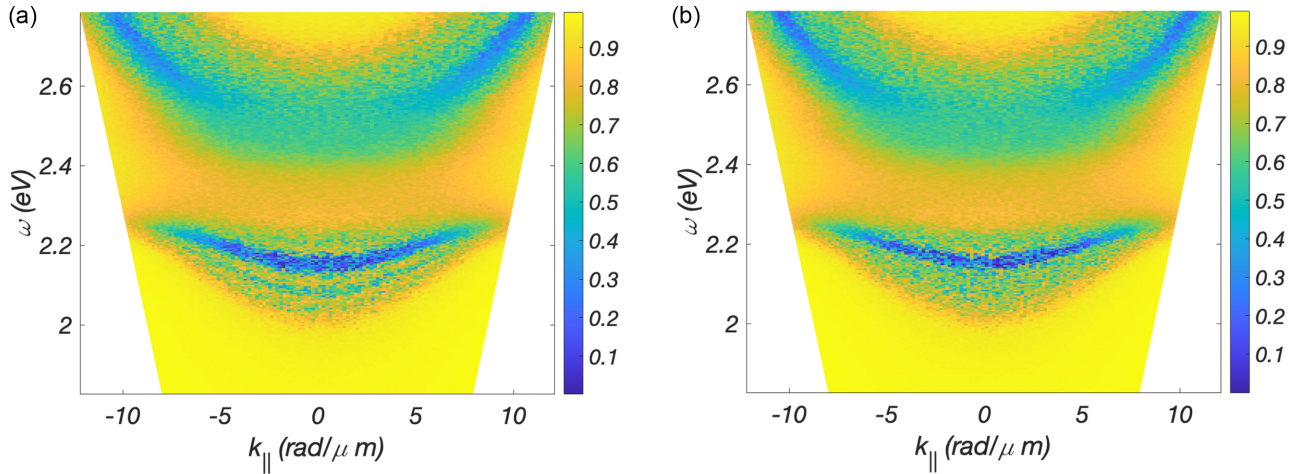


FIG. 8. Reflectance spectrum in the presence of imperfections for (a) $N = 10$ and (b) $N = 4$, that is, for 20 and 8 cavities, respectively, for the topological configuration.

Since we consider resonant conditions, in Fig. 6(b) the edge states are distanced precisely by 2Ω .

For varying angle of incidence, we observe in Fig. 7(b) the persistence of these edge states which remain confined within the corresponding band gaps. For clarity, we have highlighted the energy of these states with white markers, whereas the red dots correspond to the bulk states. In accordance with our previous analysis, also for the topological configuration the band gap associated with the lower polariton bands closes for large angles. This is a consequence of the large excitonic component of the polaritons. On the other hand, the gap separating the two upper bands slightly increases at large angles as polaritons become predominantly photonic.

Finally, in Fig. 7(c) we show the distribution of the wave function for the edge state along the cavities. The wave function is only nonzero for the A cavities, whereas it vanishes for the B cavities. The amplitude of the wave function in the A cavities decays exponentially with the index site i . At each site, the state of the polariton retains the maximal coupling between the excitons and photons, that is, the Hopfield coefficients equal to $1/2$. The distribution of the amplitude of the wave function predicted by the tight-binding model for exciton-polaritons agrees remarkably well with the electric field intensity obtained with the TMM. It captures both the vanishing of the light intensity for the B cavities and the exponential decay observed in the A cavities as a function of z . Note that the electric field is a continuous function of z where the wave function is discrete in the index site i .

The SSH model for exciton-polaritons has added remarkable physical insights to the polariton physics predicted by the TMM. However, features that extend beyond the single-particle approach of polaritons are beyond the realm of the SSH model and hence cannot be captured by this model. For instance, the breakdown of the upper polariton at normal incidence, which washes out the band gap of the upper bands, cannot be obtained within our SSH model for polaritons. This reflects the need for the dual approach: On the one hand, the TMM absent of any fitting parameters provides a powerful tool that gives the reflectance spectrum that should be experimentally observed but does not link directly to the SSH model. On the other hand, the tight-binding model allows

us to link the phenomenology of the TMM with the SSH model and provides deep physical insight, and yet it fails to contain the full complexity of the system. By combining these two approaches we obtain the complete picture of the SSH exciton-polaritons both from a pragmatic experimental point of view and in terms of the fundamental understanding of the model.

V. EXPERIMENTAL CONSIDERATIONS: ROBUSTNESS TO FABRICATION IMPERFECTIONS

In practice, there are experimental considerations that may limit the realization of the SSH array of polaritons that require discussion. First, there are incoherent processes such as photon leaking, nonradiative losses of the excitons, and coupling to additional excitonic modes. Second, there is an inability to produce mirrors with uniform widths and cavities with different lengths. Finally, there are limitations to realizing a large number of cavities, that is, finite-size effects.

In our TMM formalism, we have included the experimental values of the refractive index of the active layer; this includes all of the incoherent matter processes. On the other hand, the leaking of the photons is naturally included and arises as a broadening of the photonic lines. Our results discussed previously demonstrate that the SSH for exciton-polaritons is very robust to these effects. The topological effects for the lower polariton bands are well defined at all incident angles. For the upper polaritons, the breaking of the quasiparticle picture leads to a blurred region where the edge modes are hardly visible; however, with the opening of the angle these states become well defined. In both cases, we have found a very good agreement with the SSH polaritons treated at the single-particle level.

To study the effects of fabrication imperfections, we add a random and different error to all of the widths of both the mirrors and cavities. Experimentally, we estimate that the mirrors and cavities can be realized within an error of circa 4 nm, and thus we add an error for the fabrication of the mirrors of 5%; that is, we take $L_{M,\text{even/odd}}^i = L_{M,\text{even/odd}}^0 + \delta L_{M,\text{even/odd}}^i$, where $L_{M,\text{even/odd}}^0$ is the length of the mirrors discussed previously and $\delta L_{M,\text{even/odd}}^i$ is a random number taken to be different for

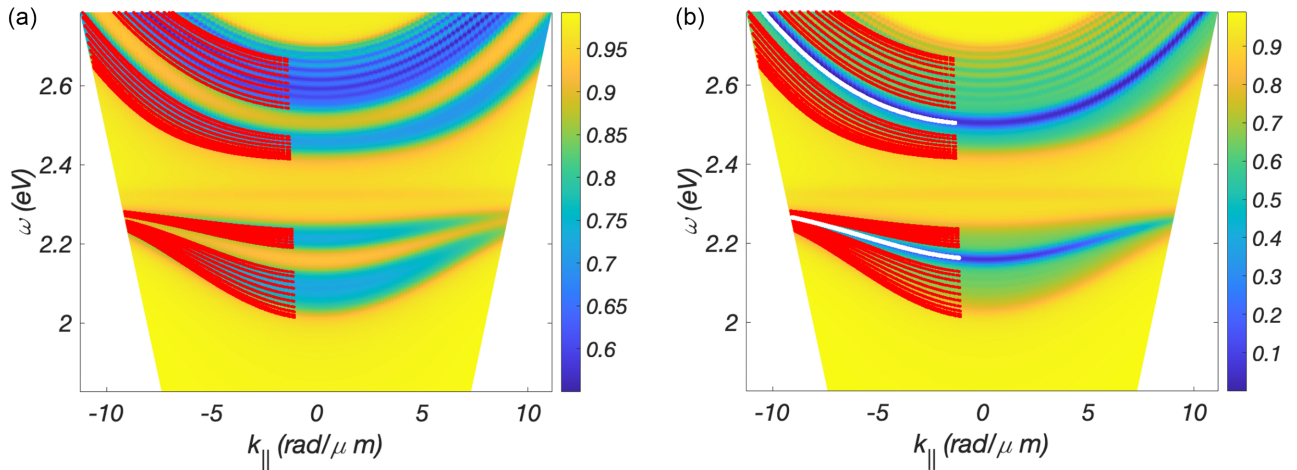


FIG. 9. s -polarized reflectance for the one-dimensional lattice of cavities containing a material with ideal excitonic response. (a) Trivial and (b) topological configuration.

each site i . We also consider an error for the cavity lengths $L_i^c = L_0^c + \delta L_i$ with $L_0^c = 140$ nm and an error of δL_i in the range $(-3.5, 3.5)$ nm, again, different for each cavity.

The reflectance spectrum adding these fabrication imperfections for an array of 20 cavities is shown in Fig. 8(a) for the topological configuration. We obtain a reflectance that closely resembles the uniform case in Fig. 5. This indicates that our proposal is indeed robust to defects in the experimental procedure that may produce mirrors and cavities with small errors in their widths.

Finally, we study the reflectance spectrum for a set of eight cavities, that is, $N = 4$ dimers; here we also retain the fabrication imperfections discussed above together with the experimental absorption spectrum of the organic molecules. The reflectance is shown in Fig. 8(b); we observe clearly the edge mode of the lower band, whereas the edge mode of the upper band becomes distinguishable at large angles. Note that Fig. 8(b) captures all the relevant features of Figs. 5 and 7(b).

Our findings allow us to conclude that our experimental proposal is robust to the underlying complexity of the exciton spectrum, inherent fabrication errors, and limited number of cavities. Therefore it stands as a promising platform to study the SSH model for organic polaritons at room temperature.

VI. IDEAL EXCITONS

Let us turn our attention to the study of ideal excitons. Here, the absorption spectrum of the active layer is single peaked, and the incoherent processes coming from the vibronic coupling are removed. This scenario is more commonly found in inorganic semiconductors, where however, incoherent processes from different microscopic origins may break the quasiparticle picture of the upper polariton [81]. The imaginary part of the refractive index is shown in Fig. 2 with the dashed blue curve, and it consists of a single narrow peak centered around $\omega \approx 2.32$ eV with an oscillatory strength of $2\Omega = 0.33$ eV and a small exciton broadening of $\gamma_X = 0.025$ eV.

In Fig. 9 we calculate the s -polarized reflectance for the trivial and topological configurations of the one-dimensional

lattice where the organic material has been replaced by one with Lorentzian excitonic response. Figure 9(a) corresponds to the trivial configuration and closely resembles Fig. 7(a). However, in this case, the upper branches are well defined even at normal incidence, and the four polariton branches are clearly visible. As expected, in the absence of the matter incoherent processes, the two edge states existing in the topological configuration appear well defined for all incident angles, as shown in Fig. 9(b).

VII. PERSPECTIVES AND CONCLUSIONS

Frenkel polaritons offer a tunable platform to realize topological phases of light and matter. The ability to produce topological states at ambient conditions is a necessary condition to deliver their promise for technological applications such as integrated quantum optical circuits, nonlinear light, and chiral and topological lasers.

Moreover, our proposal opens up opportunities for the designing of 2D and 3D topological phases by exploiting the free lateral sides of the cavity array [82].

In this paper, we have studied a one-dimensional lattice of nanocavities filled with a dye-doped polymer strongly coupled to light. By using two approaches, we have demonstrated the direct analogy between the polariton band structure of the lattice and the one-dimensional SSH model. First, we have calculated the propagation of the light field across the lattice by using the transfer matrix method. The spectra strongly depend on the configuration of the lattice: In the *trivial* phase we observed four polariton bands, namely, two lower bands below the exciton energy separated by a band gap and two upper bands above the exciton energy also distanced by a band gap; conversely, in the topological phase, we obtained two polariton states whose dispersion falls within the band gaps and whose electric field intensity localizes around the edge cavity, exponentially decaying within the lattice. In addition, we unveiled the role of the vibrational modes and fabrication imperfections. While the system is very robust to the latter, the breakdown of the

quasiparticle picture dramatically influences the emergence of the topological edge modes that appear above the bare exciton energy.

We complemented our analysis with an effective tight-binding model, which allows us to link the reflectance spectra with the SSH model. By combining these approaches we obtained a comprehensive understanding both from the experimentally relevant picture and with the elementary blocks of the single-particle polariton topological physics. Our work provides a valuable benchmark for future theories on lattices of Frenkel polaritons and realistic experimental implementations of the SSH model for Frenkel polaritons under ambient conditions.

ACKNOWLEDGMENTS

We thank Iacopo Carusotto for valuable discussions. G.P. acknowledges financial support from UNAM DGAPA PAPIIT Grant No. IN104522 and CONACyT Projects No. 1564464 and No. 1098652. H.A.L.-G. acknowledges financial support from UNAM DGAPA PAPIIT Grants No. IA103621 and No. IA107023. G.P., A.C.-G., and H.A.L.-G. acknowledge financial support from UNAM DGAPA PAPIIME PE101223. A.C.-G. acknowledges financial support from UNAM DGAPA PAPIIT Grants No. IN108620 and No. IA101923. C.L.O.-R. acknowledges financial support from UNAM DGAPA PAPIIT Grant No. IG100521.

- [1] D. G. Lidzey, D. D. C. Bradley, M. S. Skolnick, T. Virgili, S. Walker, and D. M. Whittaker, Strong exciton-photon coupling in an organic semiconductor microcavity, *Nature (London)* **395**, 53 (1998).
- [2] S. Kéna-Cohen and S. R. Forrest, Room-temperature polariton lasing in an organic single-crystal microcavity, *Nat. Photonics* **4**, 371 (2010).
- [3] T. Cookson, K. Georgiou, A. Zasedatelev, R. T. Grant, T. Virgili, M. Cavazzini, F. Galeotti, C. Clark, N. G. Berloff, D. G. Lidzey, and P. G. Lagoudakis, A yellow polariton condensate in a dye filled microcavity, *Adv. Opt. Mater.* **5**, 1700203 (2017).
- [4] J. D. Plumhof, T. Stöferle, L. Mai, U. Scherf, and R. F. Mahrt, Room-temperature Bose–Einstein condensation of cavity exciton–polaritons in a polymer, *Nat. Mater.* **13**, 247 (2014).
- [5] F. Scafrimuto, D. Urbonas, U. Scherf, R. F. Mahrt, and T. Stöferle, Room-temperature exciton-polariton condensation in a tunable zero-dimensional microcavity, *ACS Photonics* **5**, 85 (2018).
- [6] S. Betzold, M. Dusel, O. Kyriienko, C. P. Dietrich, S. Klemmt, J. Ohmer, U. Fischer, I. A. Shelykh, C. Schneider, and S. Höfling, Coherence and interaction in confined room-temperature polariton condensates with Frenkel excitons, *ACS Photonics* **7**, 384 (2020).
- [7] G. Lerario, A. Fieramosca, F. Barachati, D. Ballarini, K. S. Daskalakis, L. Dominici, M. De Giorgi, S. A. Maier, G. Gigli, S. Kéna-Cohen, and D. Sanvitto, Room-temperature superfluidity in a polariton condensate, *Nat. Phys.* **13**, 837 (2017).
- [8] K. S. Daskalakis, S. A. Maier, R. Murray, and S. Kéna-Cohen, Nonlinear interactions in an organic polariton condensate, *Nat. Mater.* **13**, 271 (2014).
- [9] T. Yagafarov, D. Sannikov, A. Zasedatelev, K. Georgiou, A. Baranikov, O. Kyriienko, I. Shelykh, L. Gai, Z. Shen, D. Lidzey, and P. Lagoudakis, Mechanisms of blueshifts in organic polariton condensates, *Commun. Phys.* **3**, 18 (2020).
- [10] P. Vasa, R. Pomraenke, S. Schwieger, Yu. I. Mazur, V. Kunets, P. Srinivasan, E. Johnson, J. E. Kihm, D. S. Kim, E. Runge, G. Salamo, and C. Lienau, Coherent Exciton–Surface-Plasmon-Polariton Interaction in Hybrid Metal-Semiconductor Nanostructures, *Phys. Rev. Lett.* **101**, 116801 (2008).
- [11] A. I. Väkeväinen, R. J. Moerland, H. T. Rekola, A. P. Eskelinen, J. P. Martikainen, D. H. Kim, and P. Törmä, Plasmonic surface lattice resonances at the strong coupling regime, *Nano Lett.* **14**, 1721 (2014).
- [12] M. Ramezani, M. Berghuis, and J. G. Rivas, Strong light–matter coupling and exciton-polariton condensation in lattices of plasmonic nanoparticles, *J. Opt. Soc. Am. B* **36**, E88 (2019).
- [13] S. Wang, Q. Le-Van, F. Vaianella, B. Maes, S. Eizagirre Barker, R. H. Godiksen, A. G. Curto, and J. Gomez Rivas, Limits to strong coupling of excitons in multilayer WS₂ with collective plasmonic resonances, *ACS Photonics* **6**, 286 (2019).
- [14] Y. Zakharko, M. Rother, A. Graf, B. Hähnlein, M. Brohmann, J. Pezoldt, and J. Zaumseil, Radiative pumping and propagation of plexcitons in diffractive plasmonic crystals, *Nano Lett.* **18**, 4927 (2018).
- [15] M. De Giorgi, M. Ramezani, F. Todisco, A. Halpin, D. Caputo, A. Fieramosca, J. Gomez-Rivas, and D. Sanvitto, Interaction and coherence of a plasmon–exciton polariton condensate, *ACS Photonics* **5**, 3666 (2018).
- [16] M. Wei, S. K. Rajendran, H. Ohadi, L. Tropic, M. C. Gather, G. A. Turnbull, and I. D. W. Samuel, Low-threshold polariton lasing in a highly disordered conjugated polymer, *Optica* **6**, 1124 (2019).
- [17] D. Ballarini, M. De Giorgi, S. Gambino, G. Lerario, M. Mazzeo, A. Genco, G. Accorsi, C. Giansante, S. Colella, S. D’Agostino, P. Cazzato, D. Sanvitto, and G. Gigli, Polariton-induced enhanced emission from an organic dye under the strong coupling regime, *Adv. Opt. Mater.* **2**, 1076 (2014).
- [18] L. Mazza, S. Kéna-Cohen, P. Michetti, and G. C. La Rocca, Microscopic theory of polariton lasing via vibronically assisted scattering, *Phys. Rev. B* **88**, 075321 (2013).
- [19] J. Zhao, A. Fieramosca, R. Bao, W. Du, K. Dini, R. Su, J. Feng, Y. Luo, D. Sanvitto, T. C. H. Liew, and Q. Xiong, Nonlinear polariton parametric emission in an atomically thin semiconductor based microcavity, *Nat. Nanotechnol.* **17**, 396 (2022).
- [20] J. Wu, R. Su, A. Fieramosca, S. Ghosh, J. Zhao, T. C. H. Liew, and Q. Xiong, Perovskite polariton parametric oscillator, *Adv. Photonics* **3**, 055003 (2021).
- [21] A. S. Kuznetsov, G. Dagvadorj, K. Biermann, M. H. Szymanska, and P. V. Santos, Dynamically tuned arrays of polariton parametric oscillators, *Optica* **7**, 1673 (2020).
- [22] E. Eizner, L. A. Martínez-Martínez, J. Yuen-Zhou, and S. Kéna-Cohen, Inverting singlet and triplet excited states using strong light-matter coupling, *Sci. Adv.* **5**, eaax4482 (2019).
- [23] K. Stranius, M. Hertzog, and K. Börjesson, Selective manipulation of electronically excited states through strong light–matter interactions, *Nat. Commun.* **9**, 2273 (2018).
- [24] J. Keeling and S. Kéna-Cohen, Bose–Einstein condensation of exciton-polaritons in organic microcavities, *Annu. Rev. Phys. Chem.* **71**, 435 (2020).

- [25] M. Sánchez-Barquilla, A. I. Fernández-Domínguez, J. Feist, and F. J. García-Vidal, A theoretical perspective on molecular polaritons, *ACS Photonics* **9**, 1830 (2022).
- [26] B. Liu, V. M. Menon, and M. Y. Sfeir, The role of long-lived excitons in the dynamics of strongly coupled molecular polaritons, *ACS Photonics* **7**, 2292 (2020).
- [27] M. Du and J. Yuen-Zhou, Catalysis by Dark States in Vibropolaritonic Chemistry, *Phys. Rev. Lett.* **128**, 096001 (2022).
- [28] Y. A. García Jomaso, B. Vargas, D. Ley Domínguez, C. L. Ordoñez-Romero, H. A. Lara-García, A. Camacho-Guardian, and G. Pirruccio, Fate of the upper polariton: Breakdown of the quasiparticle picture in the continuum, *Phys. Rev. B* **107**, L081302 (2023).
- [29] T. Ozawa, H. M. Price, A. Amo, N. Goldman, M. Hafezi, L. Lu, M. C. Rechtsman, D. Schuster, J. Simon, O. Zilberberg, and I. Carusotto, Topological photonics, *Rev. Mod. Phys.* **91**, 015006 (2019).
- [30] L. Lu, J. D. Joannopoulos, and M. Soljačić, Topological photonics, *Nat. Photonics* **8**, 821 (2014).
- [31] T. Karzig, C.-E. Bardyn, N. H. Lindner, and G. Refael, Topological Polaritons, *Phys. Rev. X* **5**, 031001 (2015).
- [32] A. Blanco-Redondo, Topological nanophotonics: toward robust quantum circuits, *Proc. IEEE* **108**, 837 (2019).
- [33] D. Smirnova, D. Leykam, Y. Chong, and Y. Kivshar, Nonlinear topological photonics, *Appl. Phys. Rev.* **7**, 021306 (2020).
- [34] G. Harari, M. A. Bandres, Y. Lumer, M. C. Rechtsman, Y. D. Chong, M. Khajavikhan, D. N. Christodoulides, and M. Segev, Topological insulator laser: theory, *Science* **359**, eaar4003 (2018).
- [35] M. A. Bandres, S. Wittek, G. Harari, M. Parto, J. Ren, M. Segev, D. N. Christodoulides, and M. Khajavikhan, Topological insulator laser: Experiments, *Science* **359**, eaar4005 (2018).
- [36] J. Jimenez, L. Cerdan, F. Moreno, B. L. Maroto, I. García-Moreno, J. L. Lunkley, G. Muller, and S. de la Moya, Chiral organic dyes endowed with circularly polarized laser emission, *J. Phys. Chem. C* **121**, 5287 (2017).
- [37] S. Schmidt and J. Koch, Circuit QED lattices: Towards quantum simulation with superconducting circuits, *Ann. Phys. (Berlin)* **525**, 395 (2013).
- [38] L. Qi, Y. Xing, J. Cao, X.-X. Jiang, C.-S. An, A.-D. Zhu, S. Zhang, and H.-F. Wang, Simulation and detection of the topological properties of a modulated Rice-Mele model in a one-dimensional circuit-QED lattice, *Sci. China Phys. Mech. Astron.* **61**, 080313 (2018).
- [39] F. Mei, J.-B. You, W. Nie, R. Fazio, S.-L. Zhu, and L. C. Kwek, Simulation and detection of photonic Chern insulators in a one-dimensional circuit-QED lattice, *Phys. Rev. A* **92**, 041805(R) (2015).
- [40] C. Owens, A. LaChapelle, B. Saxberg, B. M. Anderson, R. Ma, J. Simon, and D. I. Schuster, Quarter-flux Hofstadter lattice in a qubit-compatible microwave cavity array, *Phys. Rev. A* **97**, 013818 (2018).
- [41] J. Cho, D. G. Angelakis, and S. Bose, Fractional Quantum Hall State in Coupled Cavities, *Phys. Rev. Lett.* **101**, 246809 (2008).
- [42] Q. Lin, X.-Q. Sun, M. Xiao, S.-C. Zhang, and S. Fan, A three-dimensional photonic topological insulator using a two-dimensional ring resonator lattice with a synthetic frequency dimension, *Sci. Adv.* **4**, eaat2774 (2018).
- [43] M. Hafezi, S. Mittal, J. Fan, A. Migdall, and J. M. Taylor, Imaging topological edge states in silicon photonics, *Nat. Photonics* **7**, 1001 (2013).
- [44] S. Mittal, J. Fan, S. Faez, A. Migdall, J. M. Taylor, and M. Hafezi, Topologically Robust Transport of Photons in a Synthetic Gauge Field, *Phys. Rev. Lett.* **113**, 087403 (2014).
- [45] S. Mittal, S. Ganeshan, J. Fan, A. Vaezi, and M. Hafezi, Measurement of topological invariants in a 2D photonic system, *Nat. Photonics* **10**, 180 (2016).
- [46] H. Wang, S. K. Gupta, B. Xie, and M. Lu, Topological photonic crystals: A review, *Front. Optoelectron.* **13**, 50 (2020).
- [47] L. Lu, C. Fang, L. Fu, S. G. Johnson, J. D. Joannopoulos, and M. Soljačić, Symmetry-protected topological photonic crystal in three dimensions, *Nat. Phys.* **12**, 337 (2016).
- [48] L.-H. Wu and X. Hu, Scheme for Achieving a Topological Photonic Crystal by Using Dielectric Material, *Phys. Rev. Lett.* **114**, 223901 (2015).
- [49] S. A. Skirlo, L. Lu, Y. Igarashi, Q. Yan, J. Joannopoulos, and M. Soljačić, Experimental Observation of Large Chern Numbers in Photonic Crystals, *Phys. Rev. Lett.* **115**, 253901 (2015).
- [50] S. Raghu and F. D. M. Haldane, Analogs of quantum-Hall-effect edge states in photonic crystals, *Phys. Rev. A* **78**, 033834 (2008).
- [51] N. Malkova, I. Hromada, X. Wang, G. Bryant, and Z. Chen, Observation of optical Shockley-like surface states in photonic superlattices, *Opt. Lett.* **34**, 1633 (2009).
- [52] A. V. Poshakinskiy, A. N. Poddubny, L. Pilozzi, and E. L. Ivchenko, Radiative Topological States in Resonant Photonic Crystals, *Phys. Rev. Lett.* **112**, 107403 (2014).
- [53] U. Kuhl and H.-J. Stöckmann, Microwave Realization of the Hofstadter Butterfly, *Phys. Rev. Lett.* **80**, 3232 (1998).
- [54] W. Hu, J. C. Pillay, K. Wu, M. Pasek, P. P. Shum, and Y. D. Chong, Measurement of a Topological Edge Invariant in a Microwave Network, *Phys. Rev. X* **5**, 011012 (2015).
- [55] X. Cheng, C. Jouvaud, X. Ni, S. H. Mousavi, A. Z. Genack, and A. B. Khanikaev, Robust reconfigurable electromagnetic pathways within a photonic topological insulator, *Nat. Mater.* **15**, 542 (2016).
- [56] B. M. Anderson, R. Ma, C. Owens, D. I. Schuster, and J. Simon, Engineering Topological Many-Body Materials in Microwave Cavity Arrays, *Phys. Rev. X* **6**, 041043 (2016).
- [57] C. Poli, M. Bellec, U. Kuhl, F. Mortessagne, and H. Schomerus, Selective enhancement of topologically induced interface states in a dielectric resonator chain, *Nat. Commun.* **6**, 6710 (2015).
- [58] E. I. Rosenthal, N. K. Ehrlich, M. S. Rudner, A. P. Higginbotham, and K. W. Lehnert, Topological phase transition measured in a dissipative metamaterial, *Phys. Rev. B* **97**, 220301(R) (2018).
- [59] H. Zhao, P. Miao, M. H. Teimourpour, S. Malzard, R. El-Ganainy, H. Schomerus, and L. Feng, Topological hybrid silicon microlasers, *Nat. Commun.* **9**, 981 (2018).
- [60] L. Xin, Y. Siyuan, L. Harry, L. Minghui, and C. Yanfeng, Topological mechanical metamaterials: A brief review, *Curr. Opin. Solid State Mater. Sci.* **24**, 100853 (2020).
- [61] H. N. S. Krishnamoorthy, Z. Jacob, E. Narimanov, I. Kretzschmar, and V. M. Menon, Topological transitions in metamaterials, *Science* **336**, 205 (2012).
- [62] F. Bleckmann, Z. Cherpakova, S. Linden, and A. Alberti, Spectral imaging of topological edge states in plasmonic waveguide arrays, *Phys. Rev. B* **96**, 045417 (2017).

- [63] S. Kruk, A. Slobozhanyuk, D. Denkova, A. Poddubny, I. Kravchenko, A. Miroschnichenko, D. Neshev, and Y. Kivshar, Edge states and topological phase transitions in chains of dielectric nanoparticles, *Small* **13**, 1603190 (2017).
- [64] C. W. Ling, M. Xiao, C. T. Chan, S. F. Yu, and K. H. Fung, Topological edge plasmon modes between diatomic chains of plasmonic nanoparticles, *Opt. Express* **23**, 2021 (2015).
- [65] A. Poddubny, A. Miroschnichenko, A. Slobozhanyuk, and Y. Kivshar, Topological Majorana states in zigzag chains of plasmonic nanoparticles, *ACS Photonics* **1**, 101 (2014).
- [66] A. P. Slobozhanyuk, A. N. Poddubny, A. E. Miroschnichenko, P. A. Belov, and Y. S. Kivshar, Subwavelength Topological Edge States in Optically Resonant Dielectric Structures, *Phys. Rev. Lett.* **114**, 123901 (2015).
- [67] E. Kim, X. Zhang, V. S. Ferreira, J. Banker, J. K. Iverson, A. Sipahigil, M. Bello, A. González-Tudela, M. Mirhosseini, and O. Painter, Quantum Electrodynamics in a Topological Waveguide, *Phys. Rev. X* **11**, 011015 (2021).
- [68] A. Ott and S.-A. Biehs, Radiative heat flux through a topological Su-Schrieffer-Heeger chain of plasmonic nanoparticles, *Phys. Rev. B* **102**, 115417 (2020).
- [69] D. D. Solnyshkov, A. V. Nalitov, and G. Malpuech, Kibble-Zurek Mechanism in Topologically Nontrivial Zigzag Chains of Polariton Micropillars, *Phys. Rev. Lett.* **116**, 046402 (2016).
- [70] P. St-Jean, V. Goblot, E. Galopin, A. Lemaître, T. Ozawa, L. Le Gratiet, I. Sagnes, J. Bloch, and A. Amo, Lasing in topological edge states of a one-dimensional lattice, *Nat. Photonics* **11**, 651 (2017).
- [71] M. Parto, S. Wittek, H. Hodaei, G. Harari, M. A. Bandres, J. Ren, M. C. Rechtsman, M. Segev, D. N. Christodoulides, and M. Khajavikhan, Edge-Mode Lasing in 1D Topological Active Arrays, *Phys. Rev. Lett.* **120**, 113901 (2018).
- [72] V. K. Kozin, I. A. Shelykh, A. V. Nalitov, and I. V. Iorsh, Topological metamaterials based on polariton rings, *Phys. Rev. B* **98**, 125115 (2018).
- [73] C. A. Downing, T. J. Sturges, G. Weick, M. Stobińska, and L. Martín-Moreno, Topological Phases of Polaritons in a Cavity Waveguide, *Phys. Rev. Lett.* **123**, 217401 (2019).
- [74] R. Su, S. Ghosh, T. C. H. Liew, and Q. Xiong, Optical switching of topological phase in a perovskite polariton lattice, *Sci. Adv.* **7**, eabf8049 (2021).
- [75] M. Dusel, S. Betzold, T. H. Harder, M. Emmerling, J. Beierlein, J. Ohmer, U. Fischer, R. Thomale, C. Schneider, S. Höfling, and S. Klemmt, Room-temperature topological polariton laser in an organic lattice, *Nano Lett.* **21**, 6398 (2021).
- [76] P. Yeh, *Optical Waves in Layered Media* (Wiley, New York, 2005).
- [77] W. C. Chew, *Waves and Fields in Inhomogeneous Media*, IEEE Press Series on Electromagnetic Waves Vol. 16 (Wiley, New York, 1999).
- [78] L. Pilozzi, D. Leykam, Z. Chen, and C. Conti, Topological photonic crystal fibers and ring resonators, *Opt. Lett.* **45**, 1415 (2020).
- [79] E. D. Palik, *Handbook of Optical Constants of Solids* (Academic, New York, 1985).
- [80] L. Pilozzi, F. A. Farrelly, G. Marcucci, and C. Conti, Machine learning inverse problem for topological photonics, *Commun. Phys.* **1**, 57 (2018).
- [81] J. Levinsen, G. Li, and M. M. Parish, Microscopic description of exciton-polaritons in microcavities, *Phys. Rev. Res.* **1**, 033120 (2019).
- [82] R. O. Umucalılar and I. Carusotto, Artificial gauge field for photons in coupled cavity arrays, *Phys. Rev. A* **84**, 043804 (2011).